Neddylation inhibition protects against ischemic brain injury

Huilin Yu
Fudan University https://orcid.org/0000-0003-2885-1408
Haiyu Luo
Fudan University
Luping Chang
Fudan University https://orcid.org/0000-0003-0596-5023
Lijing Kang
Fudan University https://orcid.org/0000-0002-6455-9335
Yongliang Cao
Fudan University
Ranran Wang
Fudan University
Xing Yang
Fudan University
Yuanbo Zhu
Fudan University
Mei-Juan Shi
Fudan University
Yue Hu
Fudan University
Zhongwang Liu
Fudan University
Wenying Fan
Fudan University https://orcid.org/0000-0002-6337-729X
Bing-Qiao Zhao (bingqiaoz@fudan.edu.cn)
Fudan University https://orcid.org/0000-0002-6155-0618

Article

Keywords: neddylation, ischemic stroke, MLN4924

Posted Date: March 11th, 2021

DOI: https://doi.org/10.21203/rs.3.rs-263656/v1

Abstract

Neddylation is a ubiquitylation-like pathway that is critical in various cellular functions by conjugating NEDD8 to target proteins. However, the roles of neddylation in stroke, remain elusive. Here, we report that NEDD8 conjugation increased after ischemic stroke and was abundantly present in neutrophils, whereas cullin-1, a key substrate of neddylation, was upregulated in endothelium. Inhibition of neddylation by MLN4924, inactivated cullin-RING E3 ligase (CRL), reduced brain infarction and improved functional outcomes. MLN4924 treatment induced accumulation of the CRL substrate NF1. Knockdown of NF1 abolished MLN4924-dependent inhibition of neutrophil trafficking. These effects were mediated through activation of endothelial P-selectin and ICAM-1. Moreover, NF1 silencing blocked MLN4924-afforded BBB protection and neuroprotection through activation of PKCδ, MARCKS and MLC in cerebral microvessels. Our results demonstrate that increased neddylation promoted neutrophil trafficking and thus exacerbated injury of the BBB and stroke outcomes. We suggest that the neddylation inhibition may be beneficial in ischemic stroke.

Introduction

Stroke continues to be a leading cause of death and the most frequent cause of disability in adults. Despite significant advances in decoding the pathophysiology of cerebral ischemia, therapeutic options for stroke are still limited. Ischemic injury to the brain rapidly triggers adhesion molecule expression on the activated endothelium[1], resulting in rolling, adhesion, and extravasation of blood-derived inflammatory cells[2]. Infiltrating inflammatory cells, including neutrophils, result in irreversible impairment of blood-brain barrier (BBB) function and tissue damage through the release of reactive oxygen species, proteolytic enzymes, and proinflammatory mediators[3–5]. However, our understanding of the links between BBB breakdown and peripheral neutrophils infiltrating the ischemic brain, is still incomplete.

Neddylation is the process of posttranslational protein modification by conjugating the ubiquitin-like protein, NEDD8 (neuronal precursor cell-expressed developmentally downregulated protein 8), to target proteins[6]. This process is catalyzed by NEDD8-activating enzyme E1 (NAE1 and UBA3), NEDD8-conjugating enzyme E2 (UBC12), and NEDD8 E3 ligase[7]. The best characterized substrates of NEDD8 are cullins[6], which are scaffold proteins for the cullin-RING E3 ubiquitin ligase (CRL)[8]. The conjugation of NEDD8 to cullins leads to the activation of CRL[9], which ubiquitinates a multitude of different proteins for targeted degradation[10]. Recently, the neddylation pathway was reported to contribute to growth of a variety of cancer cells and inflammatory responses[11, 12]. In contrast, inhibition of neddylation by MLN4924, which is a small molecule inhibitor of NAE, suppressed tumor growth, reduced inflammation and prevented atherogenesis[13, 14]. However, the role of neddylation in ischemic stroke has not been addressed so far.

Using a mouse model of focal transient cerebral ischemia, we show that neddylation was upregulated in the peri-infarct cortex after stroke and was abundantly expressed in neutrophils. Treatment with the

neddylation inhibitor MLN4924 reduced brain infarction and improved neurological functions. We also demonstrated that MLN4924-afforded neuroprotection was mediated via anti-inflammatory and BBB-protective effects involving the accumulation of CRL substrate neurofibromatosis 1 (NF1).

Results

Neddylation pathway is activated in the brain after ischemic stroke. To explore the function of the neddylation pathway in ischemic stroke, we subjected mice to 1-hour transient focal cerebral ischemia and examined brains at 3, 6, 12 and 24 hours. We found that the global protein neddylation in brain lysates were increased 3 hours post stroke, reached a peak around 12 hours, and continued over 24 hours (Fig. 1a, b). Using a specific NEDD8 antibody that recognizes NEDD8-conjugated proteins, we confirmed that NEDD8 was upregulated in the peri-infarct cortex at 12 hours after stroke compared to sham-operated brains (Fig. 1c). In the ischemic cortex, NEDD8 was abundantly expressed on $Ly6G^+$ neutrophils inside the blood vessels and parenchyma (Fig. 1d), suggesting that NEDD8 may play a role in neutrophil extravasation from blood vessels and consequent BBB impairment after ischemia. The increased protein level of NEDD8 was accompanied by upregulation of the NEDD8-activating enzyme E1-NAE subunits (NAE1 and UBA3) and NEDD8-conjugating enzyme E2 (UBC12) at 12 hours after stroke (Fig. 1e-h). The best characterized substrates of neddylation are cullin-family proteins[7]. Therefore, we asked whether cullin neddylation might change after stroke. We observed a marked 5.5-fold increase in NEDD8-cullin-1 conjugation in the ischemic cortex (Fig. 1i-j). Immunostaining of brain sections showed that cullin-1 was upregulated in CD31-positive microvessels (Fig. 1k). Taken together, these data indicate that ischemic stroke induced protein neddylation.

Inhibition of neddylation by MLN4924 reduces ischemic brain damage. To address whether neddylation plays an active role in ischemic stroke, we inhibited the neddylation pathway by the specific NAE inhibitor MLN4924[15]. Treatment with MLN4924 significantly reduced cullin-1 neddylation (Fig. 2a and Supplementary Fig. 1a), showing the inactivation of CRL. Compared with the vehicle controls, injection of MLN4924 resulted in a 43.8% reduction of infarct volume at 24 hours after stroke (Fig. 2b, c). MLN4924 - treated mice had significant improvements in functional outcomes, as shown by forelimb force and rotarod latency (Fig. 2d, e). Next, we investigated whether the neuroprotective effect of MLN4924 is mediated by an apoptotic pathway. Western blot analysis showed that MLN4924 treatment induced expression of the antiapoptotic protein Bcl-2 and inhibited expression of the proapoptotic proteins p53, Bax, and caspase-3 (Fig. 2f and Supplementary Fig. 2a-d). Moreover, there was a substantial reduction of $TUNEL^+$ neurons in the MLN4924-treated group compared with the control group (Fig. 2g, h).

MLN4924 blunts BBB damage after ischemic stroke. Increase in BBB permeability greatly influenced the outcome of stroke[16]. To investigate the role of MLN4924 on BBB permeability, we first analyzed Evans blue dye extravasation at 24 hours after MCAO. This experiment showed that there was a large decrease in BBB permeability in the ischemic brain in MLN4924-treated animals compared with vehicle-treated mice (Fig. 3a, b). Using *in vivo* multiphoton microscopy of intravenously injected FITC-dextran, we found

an intact BBB in sham-operated mice and an increased BBB permeability to fluorescent dextran in mice subjected to stroke (Fig. 3c, d). Treatment with MLN4924 significantly reduced BBB damage as compared with vehicle-treated animals. Similarly, mice treated with MLN4924 exhibited a substantial reduction in the extravasation of injected fluorescent BSA (Fig. 3e, f). We next studied leakage of IgG, an endogenous blood-derived protein, in the brain. Western blot analysis of IgG in vascular-depleted brain homogenates revealed that MLN4924-treated mice had a 61.8% reduction in IgG accumulation in the brain parenchyma compared with vehicle-treated mice (Fig. 3g, h). Immunostaining for IgG and the endothelial cell marker CD31 further confirmed great reduction in perivascular IgG deposits in MLN4924-treated mice (Fig. 3i and Supplementary Fig. 3a).

The permeability of BBB is impeded by endothelial junctions, which are reduced in stroke leading to the BBB breakdown[16]. We studied whether the expression of the BBB junctional proteins is altered by MLN4924 treatment in the ischemic brain. Immunoblotting of isolated brain microvessels showed that the loss of tight junction proteins ZO-1, occludin and claudin-5 as well as the adherens junction protein VE-cadherin caused by ischemia was abolished by MLN4924 treatment (Fig. 3j and Supplementary Fig. 3b-e), suggesting that MLN4924 may play an important role in the maintenance of vascular integrity.

MLN4924 reduces cerebral neutrophil invasion. Based on these findings, we searched to elucidate the underlying cause for the protective effect of MLN4924 on BBB breakdown. Because we showed that NEDD8 is abundantly expressed in neutrophils (Fig. 1d) inside the blood vessels, we determined the effect of MLN4924 on neutrophil invasion. *In vivo* multiphoton microscopy analysis of intravenously injected PE-Ly6G showed that neutrophils adhered to the microvascular endothelium and migrated into the injured brain in mice subjected to stroke (Fig. 4b), whereas neutrophils rarely adhered or extravasated in sham-operated mice. We observed that the number of adherent neutrophils and extravasation of neutrophils from blood vessels into the brain parenchyma at 12 hours after stroke were both substantially reduced in MLN4924-treated mice compared with vehicle-treated mice (Fig. 4c, d). We also found that the neutrophil rolling velocity was significantly increased in mice injected with MLN4924 (Fig. 4e).

Consistent with these observations, immunohistochemical quantification revealed significantly decreased numbers of neutrophils in the ischemic hemispheres at 24 hours after ischemic stroke in mice treated with MLN4924 (Fig. 4f, g). These results were further confirmed by western blot using an anti-Ly6G antibody (Fig. 4h). Significantly lower amount of neutrophil was observed in the ischemic brains in mice treated with MLN4924 (Fig. 4i).

Quantification of the neutrophil-specific enzyme MPO further confirmed a significant reduction in neutrophil influx into MLN4924-treated murine brain (Fig. 4j). Together, these data suggest that MLN4924 controls both the intravascular adhesion and intraparenchymal migration of neutrophils.

In line with these findings, we found that the mRNA expression levels of neutrophil chemotactic chemokines and chemokine receptor, including CXCL1, CX3CL1, CCL2, and CCR1[17–20], were significantly lower in MLN4924-treated mice than in controls (Fig. 4k-n), suggesting that the reduced accumulation of

neutrophils in MLN4924-treated mice may cause by decreased recruitment. In addition, proinflammatory cytokine concentrations of IL-6, IL-1β and TNFα were also reduced in mice treated with MLN4924 (Fig. 4o-q).

MLN4924 reduces neutrophil infiltration via NF1. NF1, a tumor suppressor, is a key substrate of CRL[21]. NF1 loss is associated with inflammation and vascular disease[22]. We tested the hypothesis that NF1 is critical for MLN4924-mediated inhibition of neutrophil trafficking. Western blot analysis showed that ischemic stroke significantly reduced NF1 expression compared with the sham-operated group (Fig. 5a and Supplementary Fig. 4a). In contrast, injection of MLN4924 preserved the loss of NF1 caused by ischemia. We then hypothesized that NF1 silencing by adenoviral short hairpin RNA (shRNA) administration (Supplementary Fig. 5a, b) could abolish the inhibitory effect of MLN4924 on neutrophil infiltration. *In vivo* multiphoton microscopy indicated that NF1 silencing decreased rolling velocity, and increased neutrophil adhesion and transmigration (Fig. 5b-e) in MLN4924-treated mice at 12 hours after stroke. At 24 hours, we observed that injection of NF1 shRNA into MLN4924-treated mice caused a significant increase in MPO activity (Fig. 5f). The MLN4924-mediated decrease in proinflammatory cytokines was also reversed by NF1 silencing (Supplementary Fig. 6a-c).

Extravasation of neutrophils during inflammation is mediated through interactions between adhesion molecules on endothelium and neutrophils[23, 24]. Because NF1 was primarily present on cerebral vasculature in the ischemic brain (Fig. 5g), we hypothesized that NF1 loss may increase neutrophil extravasation in MLN4924-treated mice by regulating adhesion molecule expression on endothelia cells. Indeed, immunoblotting of isolated brain microvessels showed that the expression of P-selectin and ICAM-1 was significantly reduced in MLN4924-treated mice, whereas this reduction was reversed by NF1 silencing (Fig. 5h-k). In addition, MLN4924 treatment did not change the expression of vascular cell adhesion molecule-1 (VCAM-1) (Supplementary Fig. 7a, b). When using blocking antibodies against P-selectin or using anti-ICAM-1 antibodies, we observed a significant reduction in the numbers of neutrophils in the ischemic brain of mice treated with MLN4924 and NF1 shRNA (Fig. 5l, m).

NF1 mediates MLN4924-afforded BBB protection via activation of PKCδ signals. We next studied the role of NF1 inhibition by shRNA silencing on the protection of BBB with MLN4924 treatment. We observed that NF1 silencing increased BBB permeability (Fig. 6a, b) and extravascular accumulation of serum IgG (Fig. 6c, d) in mice treated with MLN4924; this was accompanied by extended infarct volume (Fig. 6e, f) and exacerbated neurological functions (Fig. 6g, h).

As NF1 was reported to regulate PKCδ activity[25], and PKCδ can be activated by ischemia[26], we next studied whether NF1 silencing abolished the protective effect of MLN4924 against BBB damage through PKCδ. Western blot analysis of isolated brain microvessels showed that ischemia-induced phosphorylation of PKCδ was inhibited by MLN4924 treatment, and these effects were reversed by silencing NF1 (Fig. 6i, j). Similarly, NF1 silencing efficiently reversed MLN4924-mediated inactivation of MARCKS protein (Fig. 6k, l), a well-recognized substrate for PKC[27]. Because MARCKS is a CaM-binding protein[28], we further studied the effects of MLN4924 treatment and NF1 silencing on the CaM-dependent

phosphorylation of MLC (pMLC), which has been implicated in endothelial barrier integrity[29]. Isolated microvessels from the ischemic brain of MLN4924-treated mice exhibited decreased pMLC compared with vehicle-treated mice (Fig. 6m, n). However, the decrease in pMLC caused by MLN4924 treatment was abolished by silencing NF1. We then injected the PKCδ inhibitor rottlerin in mice subjected to ischemia and coadministration of MLN4924 with NF1 shRNA. Rottlerin substantially reduced NF1 silencing-mediated increase in BBB permeability in MLN4924-treated mice (Fig. 6o, p). Together, these data indicate that NF1 silencing blunted MLN4924-provided BBB protection by inducing PKCδ activation.

Discussion

In this study, we found that neddylation was upregulated in the brain and active in intravascular and intraparenchymal neutrophils after transient focal ischemia in mice. We demonstrated that inhibition of neddylation by the NAE inhibitor MLN4924 improved stroke outcomes by reducing neutrophil infiltration, attenuating BBB damage and infarct volume and improving neurological functions. Furthermore, we show that MLN4924 reduced both neutrophil extravasation and BBB breakdown through attenuation of NEDD8 conjugation to cullin-1, and our data suggest that this is the result of a marked upregulation of the NF1 signals.

Neutrophils are the first line of innate immune defense against invading pathogens[30], but they also contribute to endothelial damage and tissue destruction by releasing reactive oxygen species, proteases, and proinflammatory mediators[3]. Our data show expression of vascular adhesion molecules and the accumulation of $NEDD8^+$ neutrophils in the ischemic brain after stroke, suggesting that NEDD8-mediated neutrophil trafficking may cause BBB damage and inflammation. Inhibiting neddylation using a small-molecule inhibitor MLN4924 reduced neutrophil infiltration and proinflammatory cytokine production. MLN4924 was shown to cause accumulation of a multitude of different proteins by inactivating CRL[31]. In this study, we found that MLN4924 significantly increased the accumulation of NF1, a CRL substrate, whereas NF1 silencing by adenoviral short hairpin RNA administration induced the expression of P-selectin and ICAM-1 in brain microvessels to increase neutrophil extravasation in MLN4924-treated mice, suggesting that the anti-inflammatory effect of MLN4924 may involve NF1. Importantly, we show here that NF1 silencing-induced increase in neutrophil infiltration in MLN4924-treated mice could be rescued by either blocking antibodies against P-selectin or anti-ICAM-1 antibodies, suggesting the need of a specific interaction between activated neutrophils and injured endothelial cells for induction of neutrophil transmigration.

Inflammation in cerebral vessels contributes to BBB disruption[32, 33], and high BBB permeability correlates with infarction growth[34] and poor clinical prognosis after stroke[35, 36]. The present study demonstrated that MLN4924 treatment preserved BBB integrity and thereby reduced BBB permeability after cerebral ischemia. These BBB-protective effects of MLN4924 were accompanied by reduced apoptotic neurons and smaller brain infarctions and less severe neurologic deficits. Furthermore, we show that MLN4924-offered protection against BBB breakdown is depended on its action on NF1. We then attempted to

provide information regarding the signaling mechanisms by which NF1 mediated the BBB protection of MLN4924. Our data indicated a robust downregulation of ischemia-induced activation of PKCδ-MARCKS-MLC pathway upon MLN4924 treatment, and silencing NF1 promoted the activation of PKCδ pathway again and blocked MLN4924-afforded BBB protection. However, in addition to NF1-mediated inactivation of PKCδ pathway, multiple other CRL substrates may also contribute to the effects of MLN4924.

In summary, our study has uncovered a crucial role for protein neddylation in regulating cerebral ischemia. Because its impressive anticancer efficacy, MLN4924 is currently in phase I/II clinical trials for the treatment of several cancers[37]. Our data demonstrated that the neddylation inhibitor MLN4924 protected the brain against ischemic injury by attenuating neutrophil extravasation into brain and maintaining BBB integrity. We conclude that MLN4924 could represent a novel therapeutic option for ischemic stroke.

Methods

Animal stroke model. Male C57BL/6 mice (Shanghai SLAC Laboratory Animal Co. Ltd., Shanghai, China) weighing 23-26g were used in this study. All protocols for these studies were approved by the Animal Care and Use Committee of the Shanghai Medical College of Fudan University according to National Institutes of Health Guidelines Mice were anesthetized with 1-1.5% isoflurane in 30% oxygen and 70% nitrous oxide. Focal cerebral ischemia was induced by occlusion of the right middle cerebral artery (MCA) for 60 minutes with a siliconized filament[38]. Cerebral blood flow was monitored by continuous laser doppler flowmetry (Perimed, Stockholm, Sweden) to confirm induction of ischemia and reperfusion. Body temperature was maintained at 37 ± 0.5°C using a temperature control unit (World Precision Instruments, Florida) during surgery. MLN4924 (10mg/ml, 60mg/kg) or vehicle (10% 2-hydroxypropyl-β-cyclodextrin) was injected subcutaneously twice at 1 and 12 hours after MCA occlusion[39]. Adenoviral vector expressing NF1 shRNA (pDKD-CMV-Puro-U6-(NF1)-shRNA, produced by Obio Technology, Shanghai, China) or control shRNA (pDKD-CMV-Puro-U6-shRNA) (2 μl of 1.34×10^{11} plaque-forming-unit/ml) was injected into three points of cortex (coordinates: 0.3 mm anterior, 0.8 mm and 1.9 mm posterior to bregma, 3.0 mm lateral to midline, and 2.0 mm ventral to skull surface) in the right hemisphere 3 days before stroke[40]. Blocking antibodies against P-selectin (1.6 mg/kg, 553742, BD Pharmingen, San Jose, CA), anti-intercellular adhesion molecule-1 (ICAM-1) antibodies (200 μg/mouse, YN1/1.7.4, BE0020-1, Bioxcell, NH) or isotype control antibody was administered intravenously immediately before MCAO[41, 42]. Protein kinase C δ (PKCδ) inhibitor rottlerin (10 mg/kg) or vehicle (2% dimethyl sulfoxide) was injected intraperitoneally 30 minutes before stroke[43, 44].

Cranial window surgery and multiphoton microscopy. Cranial windows were prepared as we previously described[45, 46]. Mice were anaesthetized with 1-1.5% isoflurane in 30% oxygen and 70% nitrous oxide. Body temperature was maintained at 37 ± 0.5°C during surgery. After fixation in a stereotaxic head holder, a craniotomy (5 mm diameter) was created above the right somatosensory cortex (centered 2.5 mm lateral and 2.5 mm posterior to the bregma) using a high-speed micro drill. The window was closed with a

sterile cover glass. For multiphoton imaging, Olympus FluoView FVMPE-RS upright multiphoton laser-scanning system with an Olympus XL Plan N 25 × /1.05 WMP ∞/0-0.23/FN/18 dipping objective was used. Multiphoton excitation was performed using MAITAI eHPDS-OL and Spectra Physics InSight DS-OL lasers (Mai Tai, Spectra-Physics, CA). Emitted fluorescence was detected through 495–540 nm and 575-645nm bandpass filters.

For imaging of neutrophils, phycoerythrin (PE)-conjugated monoclonal Ly6G antibody (1A8 clone; 3 μg, 551461, BD Pharmingen) was intravenously injected into mice[46]. Fluorescein isothiocyanate (FITC)-dextran (0.1 ml of 10 mg/ml, 2000 KDa, Sigma-Aldrich, MO) was used to label the cerebral vasculature. Time-lapse images at 6 μm steps were acquired from 100 to 150 μm below the surface every 6 seconds for 25 minutes. The area scanned was at 900 nm excitation wavelength in a 508 × 508 μm with 512 × 512 pixel resolution. Neutrophil movement was determined by imaging of blood vessels with a diameter between 20 and 40 μm. Images reconstruction was carried out using Olympus FV 10-ASW software. Neutrophil movement analysis was performed using the IMARIS image analysis software (Bitplane AG, Zurich, Switzerland). Forty cells per animal were tracked. Adherent neutrophils were defined as the cells that were remained arrested in the microvessels for at least 30 seconds. The intravascular rolling velocity for neutrophils was calculated by determining the distance neutrophils moved between a certain time. Transmigrated neutrophils were determined in an area reaching out 75 μm to each side of a 100-μm-length vessel (representing 1.5×10^4 μm^2 tissue area).

Cerebrovascular permeability based on FITC-dextran (MW = 40 KDa, Sigma-Aldrich) leakage was analyzed as described previously[47]. In brief, time lapse imaging of FITC-dextran was acquired every 3 minutes for 30 minutes. The fluorescence of randomly chosen 20 × 20 μm^2 regions of interest within the vessel and corresponding areas within the perivascular brain parenchyma were recorded.

Measurements of Evans blue and BSA vascular leakage. At 23 hours after MCAO, mice were intravenously injected with 4 ml/kg of 4% Evans blue dye (Sigma-Aldrich). After 1 hour, mice were perfused transcardially with phosphate buffer saline (PBS), and ischemic hemispheres were weighted and placed in formamide for 72 hours. After centrifugation, the amount of extravasated Evans blue dye in the supernatants was evaluated by spectrophotometry (Thermo Scientific, MA) at 620 nm[48]. Alexa fluor 488-conjugated bovine serum albumin (BSA; 66 kDa, 50 μl of 100 mg/ml) was intravenously injected into mice 1 hour before killing[49]. Brains were collected, fixed in 4% paraformaldehyde and cryoprotected in 30% sucrose in PBS. Coronal brain sections (20 μm thick) were used for fluorescent detection. Images were acquired using an Olympus FV1000 confocal microscope and an Olympus BX 63 microscope, and extravascular BSA fluorescence in tissue sections was quantified using NIH Image J software.

Analysis of extravascular IgG deposition. Coronal brain sections were blocked with 1% BSA in PBS and incubated with goat anti-CD31 antibody (AF3628, R&D Systems, MN) overnight at 4˚C. The sections were washed and incubated with Alexa Fluor 488-conjugated donkey anti-mouse immunoglobulin G (IgG) and Alexa Fluor 594-conjugated donkey anti-goat IgG (Invitrogen, Carlsbad, CA). To quantify extravascular

deposits of IgG, the images were contrast enhanced to clearly differentiate positivity from background and quantified using the NIH Image J integrated density analysis tool.

Neurobehavioral test. Forelimb force and rotarod test were carried out by an investigator blinded to the experimental groups as described previously[46, 48]. In the forelimb force test, a grip strength meter (Bio-Seb, Vitrolles, France) was used to assess the peak force exerted by a mouse when the mouse released the forepaws from a grid. In the rotarod test, mice were placed on an accelerating rotating rotarod cylinder (Ugo Basile, Varese, Italy), and the time the mice remained on the rotarod was recorded. The speed was increased from 5 to 40 rpm within 5 minutes. Before surgery, mice were trained for 3 days.

Measurement of infarct volume and neuronal death. At 24 hours after MCAO, mice were sacrificed. The infarct area was detected by 2% triphenyl-2,3,5-tetrazolium chloride (TTC) staining and measured using the NIH Image J software in a blinded manner. Neuronal cell death in peri-infarct regions was detected using an *In Situ* Cell Death Detection Kit (11684795910, Roche, Mannheim, Germany) and mouse anti-neuronal nuclei (NeuN, MAB377, Millipore, MA) immunostaining.

Immunoblotting. Brain capillaries and capillary-depleted brain homogenates were prepared as we described previously[46, 50]. Isolated protein from brain tissues, capillaries, and capillary-depleted brain homogenates was detected by immunoblotting according to standard procedures[46, 50]. The primary antibodies used were: rabbit anti-NEDD8 (1:1000, 2754), rabbit anti-Bcl-2 (1:1000, 3498), mouse anti-p53 (1:1000, 2524), rabbit anti-Bax (1:1000, 2772), rabbit anti-Cleaved Caspase-3 (caspase-3, 1:1000, 9661), HRP-linked anti-mouse IgG (1:2000, 7076), rabbit anti-phospho-PKCδ (pPKCδ, 1:1000, 9376), rabbit anti-phospho-Myosin Light Chain (pMLC; 1:1000, 3671), rabbit anti-Myosin Light Chain (MLC, 1:1000, 3672), and rabbit anti-β-actin (1:1000, 4970, all from Cell Signaling Technology, Danvers, MA), rabbit anti-APPBP1 (NAE1, 1:1000, SAB1300843, Sigma-Aldrich), rabbit anti-UBA3 (1:1000, ab124728), rabbit anti-UBE2M/UBC12 (1:1000, ab109507), rabbit anti-occludin (1:1000, ab167161), rabbit anti-claudin5 (1:1000, ab15106), rabbit anti-CD144 (vascular endothelial cadherin, VE-cadherin; ab33168), rabbit anti-protein kinase Cδ (PKCδ, 1:1000, ab182126), rabbit anti-phospho-myristoylated alanine-rich C-kinase substrate (pMARCKS, 1:1000, ab81295,all from Abcam, Cambridge, UK), mouse anti-CUL-1 (1:1000, sc-17775), mouse anti-Neurofibromin (NF1, 1:1000, sc-376886), mouse anti-P-Selectin (1:1000, sc-8419), mouse anti-MARCKS (1:1000, sc-100777, Santa Cruz Biotechnology, Dallas, Texas), rat anti-mouse Ly6G (1:1000, 551459, BD Pharmingen), rabbit anti-Zonula occludens-1 (ZO-1; 1:1000, 617300, Invitrogen), goat anti-ICAM-1/CD54 (1:1000, AF796), goat anti-vascular cell adhesion molecule-1 (VCAM-1, 1:1000, AF643, both from R&D Systems, Minneapolis). Blots were visualized by labeling with horseradish peroxidase-conjugated anti-rabbit, anti-goat, anti-mouse, anti-rat secondary antibodies (CST) and incubation with chemiluminescent substrate (Millipore). Blots were processed and analysed with the Image Lab-5.2.1 software (Bio-Rad Laboratories, CA).

MPO activity assay. Mice were sacrificed, perfused with ice cold PBS and the brains were removed. Ipsilateral brain hemispheres were homogenized in 50 mM potassium phosphate buffer, centrifuged, and resuspended in 0.5% cetyltrimethylammonium bromide (Sigma-Aldrich) in potassium phosphate buffer.

The suspensions were sonicated for 30 seconds with 3 cycles of freeze-thaw in liquid nitrogen. After centrifugation, 40 µl of supernatant was mixed with 100 µl tetramethylbenzidine solution (Sigma-Aldrich) in a 96-well plate in duplicates. The reaction was stopped with 100 µl 2N HCl after 15 minutes. The absorbance was measured at 450 nm in a microplate reader (Bio-Tek, Vermont). Myeloperoxidase (MPO) activity was calculated using purified MPO (Sigma-Aldrich) and was expressed as units of MPO per mg protein.

Quantitative real-time polymerase chain reaction. Total RNA was isolated from brain tissue using the TRIzol kits (Invitrogen) according to the manufacturer's protocol. The polymerase chain reaction (PCR) was performed with equal amounts of cDNA in a Mastercycler ep gradient machine (Eppendorf AG 22331 Hamburg, Germany)[45]. Relative changes in gene expression levels were calculated as the ratio of target cDNA to GAPDH. The following primers were used: Chemokine (C-X-C motif) ligand 1 (CXCL1) forward 5'-ACCCAAACCGAAGTCATAGCC-3', reverse 5'-TTGTCAGAAGCCA GCGTTCA-3', CX3CL1 forward 5'-GCCATTGTCCTGGAGACGAC-3', reverse 5'-CCAAGGTGATCCCA GGTGTC-3', chemokine (C-C motif) ligand 2 (CCL2) forward 5'-GCTG-TAGTTTTTGTCA CCAAGC-3', reverse 5'-AAGGCATCACAGTCCGAGTC-3', chemokine receptor 1 (CCR1) forward 5'-ACTCTGGAAACACAGACTCACT-3', reverse 5'-GCCCACCACTCCAATGAT GA-3', GAPDH forward 5'-AGGTCGGTGTGAACGGATTT G-3', reverse 5'-TGTAGACCATGTAGTTGAGGTCA-3'.

Measurements of interleukin-6, interleukin-1β and TNF-α levels. Protein from brain tissue was extracted in radioimmunoprecipitation (RIPA) lysis buffer (Millipore) containing protease inhibitor cocktail (Roche Diagnostics, Mannheim, Germany). Protein concentration was determined by bicinchoninic acid (BCA) protein assay kit (Pierce, Rockford, IL). Quantification of interleukin (IL)-6, IL-1β and tumor necrosis factor-α (TNF-α) proteins were performed using enzyme-linked immunosorbent assay (ELISA) kits (R&D systems) according to the manufacturer's instructions.

Immunohistochemistry. Mice were deeply anaesthetized with isoflurane and perfused transcardially with PBS followed by 4% paraformaldehyde in PBS. Brains were removed and immersed in 4% paraformaldehyde and cryoprotected in 30% sucrose. Coronal sections of 20 µm thickness were prepared on a cryostat and collected on glass slides. Sections were stained according to standard immunohistochemistry procedures with the following primary antibodies: mouse anti-NEDD8 (1:200, sc-373741), mouse anti-CUL-1 (1:1000, sc-17775), mouse anti-Neurofibromin (NF1, 1:1000, sc-376886, all from Santa Cruz), rat anti-Ly6G (1:200, 551459, BD Pharmingen), goat anti-CD31 (1:200, AF3628, R&D Systems), mouse anti-neuronal nuclei (NeuN, MAB377, Millipore). The secondary antibodies used were Alexa Fluor 488-conjugated donkey anti-rat IgG, Alexa Fluor 488-conjugated donkey anti-goat IgG, Alexa Fluor 594-conjugated donkey anti-mouse IgG, Alexa Fluor 488-conjugated donkey anti-mouse IgG, Alexa Fluor 594-conjugated donkey anti-goat IgG, Alexa Fluor 647-conjugated donkey anti-goat IgG and biotin-donkey anti-mouse IgG (all from Invitrogen). DNA was stained with Hoechst 33342 (1:10000, H3570, Invitrogen). For each animal, three fields from the peri-infarct cortex in each section were obtained under × 40 objective. Images were traced (quantitative analyzed) using Image J 1.48v software. The numbers of $Ly6G^+$ neutrophils in the traced area were counted.

Statistics. All values are presented as means ± standard deviation (SD). Statistical analysis for multiple comparisons were performed in Prism 7 software using one-way ANOVA followed by Bonferroni multiple comparison test. Differences between the two groups were assessed by unpaired Student's *t*-test. A value of $P < 0.05$ was considered statistically significant.

Data Availability

All data supporting the findings of this study are available within the article and its supplementary information files or from the corresponding author upon reasonable request.

References

1. Okada, Y. et al. P-selectin and intercellular adhesion molecule-1 expression after focal brain ischemia and reperfusion. *Stroke* **25**, 202–211 (1994).
2. Ley, K., Laudanna, C., Cybulsky, M.I. & Nourshargh, S. Getting to the site of inflammation: the leukocyte adhesion cascade updated. *Nat. Rev. Immunol.* **7**, 678–689 (2007).
3. Scholz, M., Cinatl, J., Schadel-Hopfner, M. & Windolf, J. Neutrophils and the blood-brain barrier dysfunction after trauma. *Med. Res. Rev.* **27**, 401–416 (2007).
4. Cao, D.J. et al. Cytosolic DNA sensing promotes macrophage transformation and governs myocardial ischemic injury. *Circulation* **137**, 2613–2634 (2018).
5. Yepes, M. TWEAK and the central nervous system. *Mol. Neurobiol.* **35**, 255–265 (2007).
6. Xirodimas, D.P. Novel substrates and functions for the ubiquitin-like molecule NEDD8. *Biochem. Soc. Trans.* **36**, 802–806 (2008).
7. Rabut, G. & Peter, M. Function and regulation of protein neddylation. 'Protein modifications: beyond the usual suspects' review series. *EMBO Rep.* **9**, 969–976 (2008).
8. Petroski, M.D. & Deshaies, R.J. Function and regulation of cullin-RING ubiquitin ligases. *Nat. Rev. Mol. Cell Biol.* **6**, 9–20 (2005).
9. Duda, D.M. et al. Structural insights into NEDD8 activation of cullin-RING ligases: conformational control of conjugation. *Cell* **134**, 995–1006 (2008).
10. Sarikas, A., Hartmann, T. & Pan, Z.Q. The cullin protein family. *Genome. Biol.* **12**, 220 (2011).
11. Nawrocki, S.T. et al. Disrupting protein NEDDylation with MLN4924 is a novel strategy to target cisplatin resistance in ovarian cancer. *Clin. Cancer Res.* **19**, 3577–3590 (2013).
12. Jin, H.S., Liao, L., Park, Y. & Liu, Y.C. Neddylation pathway regulates T-cell function by targeting an adaptor protein Shc and a protein kinase Erk signaling. *Proc. Natl. Acad. Sci. USA* **110**, 624–629 (2013).
13. Swords, R.T. et al. Inhibition of NEDD8-activating enzyme: a novel approach for the treatment of acute myeloid leukemia. *Blood* **115**, 3796–3800 (2010).

14. Asare, Y. et al. Inhibition of atherogenesis by the COP9 signalosome subunit 5 in vivo. *Proc. Natl. Acad. Sci. USA* **114**, E2766-E2775 (2017).
15. Soucy, T.A. et al. An inhibitor of NEDD8-activating enzyme as a new approach to treat cancer. *Nature* **458**, 732–736 (2009).
16. Knowland, D. et al. Stepwise recruitment of transcellular and paracellular pathways underlies blood-brain barrier breakdown in stroke. *Neuron* **82**, 603–617 (2014).
17. Girbl, T. et al. Distinct Compartmentalization of the Chemokines CXCL1 and CXCL2 and the atypical receptor ACKR1 determine discrete stages of neutrophil diapedesis. *Immunity* **49**, 1062–1076 e1066 (2018).
18. Brauer, R. et al. MMP-19 deficiency causes aggravation of colitis due to defects in innate immune cell function. *Mucosal. Immunol.* **9**, 974–985 (2016).
19. Souto, F.O. et al. Essential role of CCR2 in neutrophil tissue infiltration and multiple organ dysfunction in sepsis. *Am. J. Respir. Crit. Care Med.* **183**, 234–242 (2011).
20. Kiyasu, Y. et al. Disruption of CCR1-mediated myeloid cell accumulation suppresses colorectal cancer progression in mice. *Cancer Lett.* **487**, 53–62 (2020).
21. Upadhyay, A. et al. E3 ubiquitin ligases neurobiological mechanisms: development to degeneration. *Front Mol. Neurosci.* **10**, 151 (2017).
22. Lasater, E.A. et al. Genetic and cellular evidence of vascular inflammation in neurofibromin-deficient mice and humans. *J. Clin. Invest.* **120**, 859–870 (2010).
23. Muller, W.A. Transendothelial migration: unifying principles from the endothelial perspective. *Immunol. Rev.* **273**, 61–75 (2016).
24. Cedervall, J., Dimberg, A. & Olsson, A.K. Tumor-induced neutrophil extracellular traps-drivers of systemic inflammation and vascular dysfunction. *Oncoimmunology* **5**, e1098803 (2016).
25. Ghoshal, P. et al. Loss of GTPase activating protein neurofibromin stimulates paracrine cell communication via macropinocytosis. *Redox Biol.* **27**, 101224 (2019).
26. Hafeez, A. et al. Reduced apoptosis by ethanol and its association with PKC-delta and Akt signaling in ischemic stroke. *Aging Dis.* **5**, 366–372 (2014).
27. Blackshear, P.J. The MARCKS family of cellular protein kinase C substrates. *J. Biol. Chem.* **268**, 1501–1504 (1993).
28. Hartwig, J.H. et al. MARCKS is an actin filament crosslinking protein regulated by protein kinase C and calcium-calmodulin. *Nature* **356**, 618–622 (1992).
29. Kuhlmann, C.R. et al. Inhibition of the myosin light chain kinase prevents hypoxia-induced blood-brain barrier disruption. *J. Neurochem.* **102**, 501–507 (2007).
30. Ley, K. et al. Neutrophils: New insights and open questions. *Sci. Immunol.* **3**(2018).
31. Tanaka, T., Nakatani, T. & Kamitani, T. Inhibition of NEDD8-conjugation pathway by novel molecules: potential approaches to anticancer therapy. *Mol. Oncol.* **6**, 267–275 (2012).

32. McColl, B.W., Rothwell, N.J. & Allan, S.M. Systemic inflammation alters the kinetics of cerebrovascular tight junction disruption after experimental stroke in mice. *J. Neurosci.* **28**, 9451–9462 (2008).
33. Yepes, M. TWEAK and Fn14 in the neurovascular unit. *Front Immunol.* **4**, 367 (2013).
34. Shen, J. et al. PDGFR-beta as a positive regulator of tissue repair in a mouse model of focal cerebral ischemia. *J. Cereb. Blood Flow Metab.* **32**, 353–367 (2012).
35. Warach, S. & Latour, L.L. Evidence of reperfusion injury, exacerbated by thrombolytic therapy, in human focal brain ischemia using a novel imaging marker of early blood-brain barrier disruption. *Stroke* **35**, 2659–2661 (2004).
36. Khatri, R., McKinney, A.M., Swenson, B. & Janardhan, V. Blood-brain barrier, reperfusion injury, and hemorrhagic transformation in acute ischemic stroke. *Neurology* **79**, S52-57 (2012).
37. Toth, J.I., Yang, L., Dahl, R. & Petroski, M.D. A gatekeeper residue for NEDD8-activating enzyme inhibition by MLN4924. *Cell Rep.* **1**, 309–316 (2012).
38. Wang, L. et al. Recombinant ADAMTS13 reduces tissue plasminogen activator-induced hemorrhage after stroke in mice. *Ann. Neurol.* **73**, 189–198 (2013).
39. Robertson, R., Germanos, M.S., Manfredi, M.G., Smith, P.G. & Silva, M.D. Multimodal imaging with (18)F-FDG PET and Cerenkov luminescence imaging after MLN4924 treatment in a human lymphoma xenograft model. *J. Nucl. Med.* **52**, 1764–1769 (2011).
40. Zhou, L. et al. Treatment of cerebral ischemia by disrupting ischemia-induced interaction of nNOS with PSD-95. *Nat. Med.* **16**, 1439–1443 (2010).
41. Asaduzzaman, M., Rahman, M., Jeppsson, B. & Thorlacius, H. P-selectin glycoprotein-ligand-1 regulates pulmonary recruitment of neutrophils in a platelet-independent manner in abdominal sepsis. *Br. J. Pharmacol.* **156**, 307–315 (2009).
42. Thomas, S.Y. et al. PLZF induces an intravascular surveillance program mediated by long-lived LFA-1-ICAM-1 interactions. *J. Exp. Med.* **208**, 1179–1188 (2011).
43. Mai, H.N. et al. Protein kinase Cdelta knockout mice are protected from cocaine-induced hepatotoxicity. *Chem. Biol. Interact* **297**, 95–108 (2019).
44. Du, Y. et al. Inhibition of PKCdelta reduces amyloid-beta levels and reverses Alzheimer disease phenotypes. *J. Exp. Med.* **215**, 1665–1677 (2018).
45. Xu, H. et al. ADAMTS13 controls vascular remodeling by modifying VWF reactivity during stroke recovery. *Blood* **130**, 11–22 (2017).
46. Kang, L. et al. Neutrophil extracellular traps released by neutrophils impair revascularization and vascular remodeling after stroke. *Nat. Commun.* **11**, 2488 (2020).
47. Wang, R. et al. Neutrophil extracellular traps promote tPA-induced brain hemorrhage via cGAS in mice with stroke. *Blood.* In Press.
48. Cai, P. et al. Recombinant ADAMTS 13 attenuates brain injury after intracerebral hemorrhage. *Stroke* **46**, 2647–2653 (2015).

49. Krueger, M., Mages, B., Hobusch, C. & Michalski, D. Endothelial edema precedes blood-brain barrier breakdown in early time points after experimental focal cerebral ischemia. *Acta Neuropathol. Commun.* **7**, 17 (2019).
50. Cao, Y. et al. ADAMTS13 maintains cerebrovascular integrity to ameliorate Alzheimer-like pathology. *PLoS Biol.* **17**, e3000313 (2019).

Figures

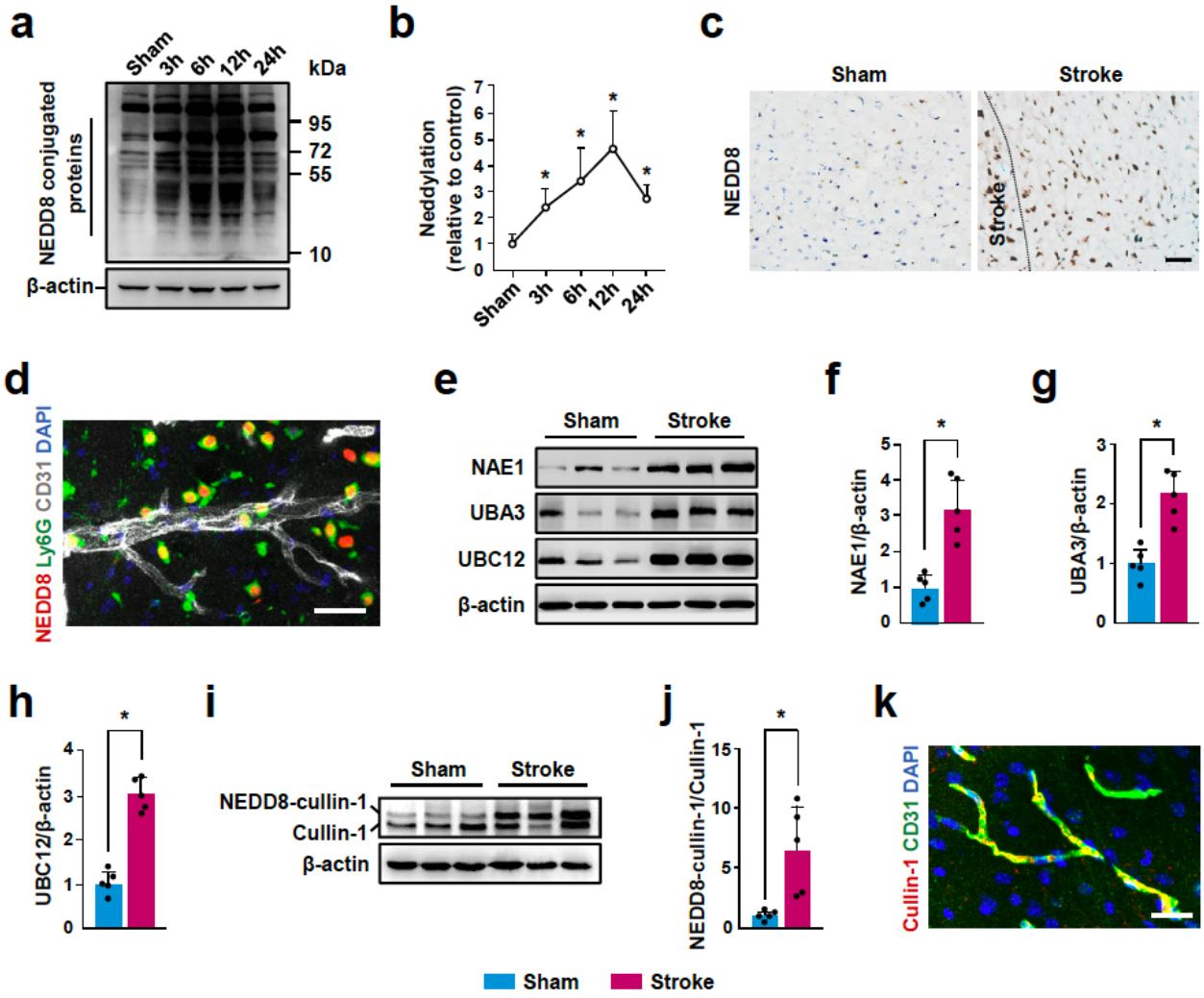

Figure 1

Neddylation pathway is upregulated after ischemic stroke. a Western blot assay for global NEDD8 conjugation in the ipsilateral hemisphere in sham-operated mice and ischemic mice at 3, 6, 12, and 24 hours following operation. b Quantitative determinations of global NEDD8 conjugation for each group (n = 5). c Representative NEDD8 immunostaining at 12 hours after stroke, compared with sham-operated

mice. Bar = 50 μm. d Representative confocal image showing NEDD8 (red) abundant co-localization with Ly6G+ neutrophils (green) in microvessels and parenchyma. White indicates CD31-positive microvessels. Nuclei were stained with DAPI (blue). Bar = 40 μm. e Western blot assay for NAE1, UBA3, and UBC12 in sham-operated mice and ischemic mice at 12 hours following operation. f-h Quantitative determinations of NAE1 (f), UBA3 (g), and UBC12 (h) for each group (n = 5). i Western blot assay for cullin-1 neddylation in sham-operated mice and ischemic mice at 12 hours following operation. j Quantitative determinations of cullin-1 neddylation for each group (n = 5). k Representative confocal image shows that cullin-1 (red) colocalized with the endothelial cell marker CD31 (green). Nuclei were stained with DAPI (blue). Bar = 20 μm. Data were analyzed using one-way ANOVA followed by Bonferroni multiple comparison test and unpaired Student's t test. Values are mean ± SD. * P < 0.05.

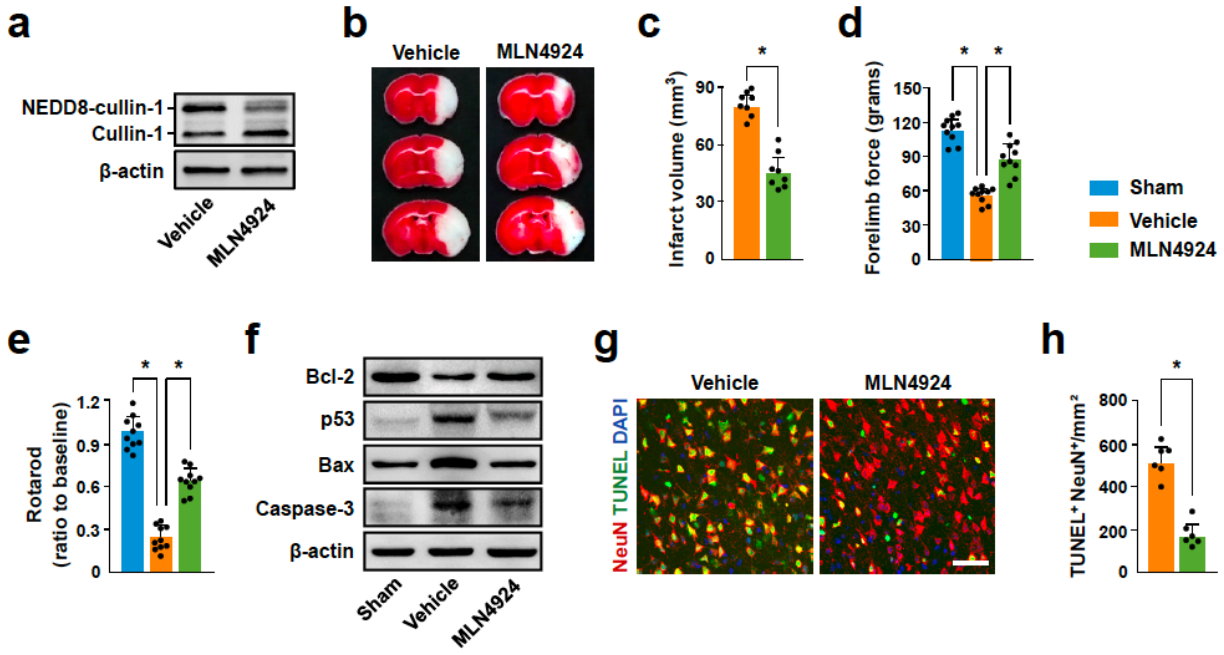

Figure 2

MLN4924 reduces ischemic cerebral injury and improves behavioral outcomes. a Inhibition of cullin-1 neddylation by MLN4924. Immunoblotting of lysates from the ipsilateral hemisphere in ischemic mice treated with vehicle or MLN4924 at 24 hours after stroke. b Representative photographs of TTC stained coronal brain sections showing smaller cerebral infarct in mice treated with MLN4924 than in mice treated with vehicle at 24 hours after stroke. c Quantitation of infarct volumes for each group (n = 8). d, e MLN4924 improved behavioral outcomes in forelimb force test (d) and rotarod test (e) (n = 10). f Western blot assay for antiapoptotic proteins Bcl-2 and proapoptotic proteins p53, Bax and caspase-3 in ischemic mice treated with vehicle or MLN4924. g, h Representative images (g) and quantification (h) of TUNEL+ neurons in ischemic mice treated with vehicle or MLN4924 (n = 6). Bar = 40 μm. Data were analyzed

using unpaired Student's t test and one-way ANOVA followed by Bonferroni multiple comparison test. Values are mean ± SD. * P < 0.05.

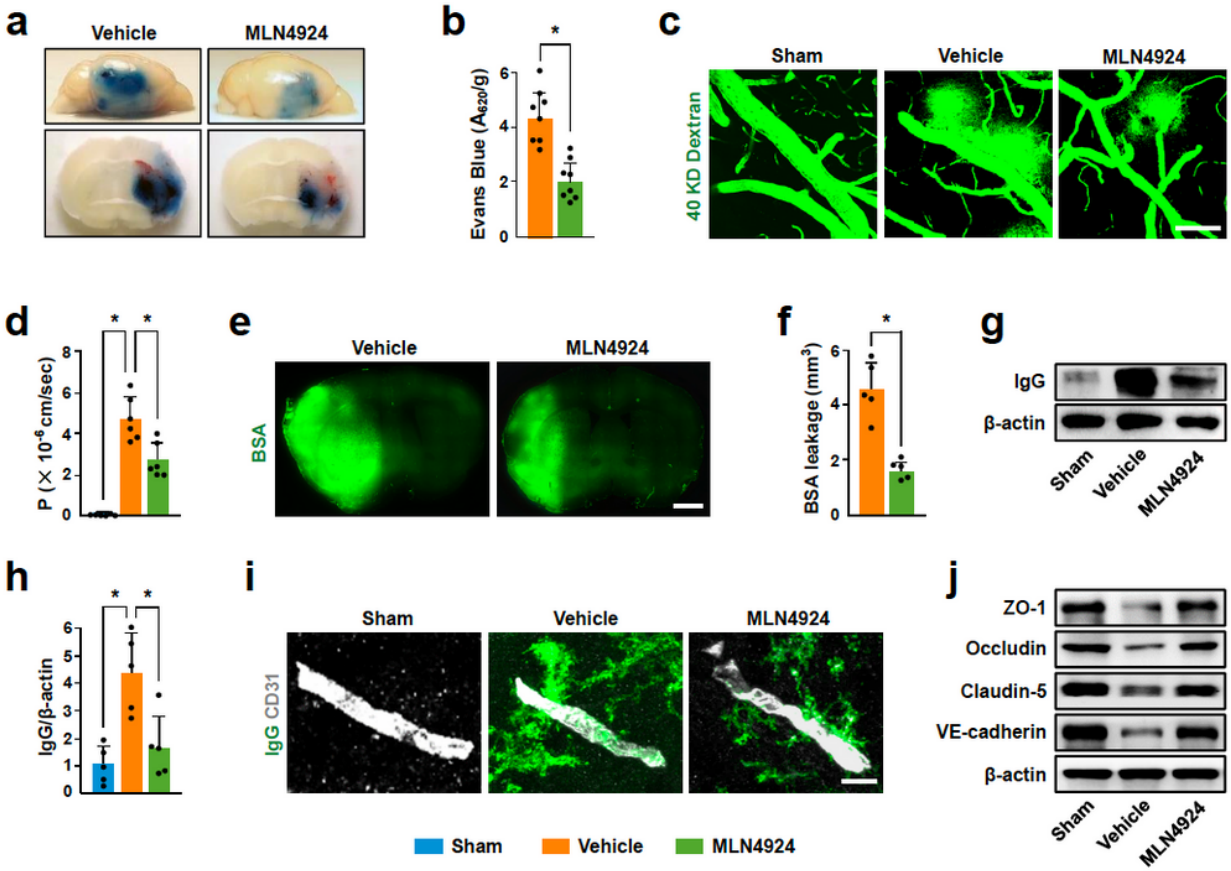

Figure 3

MLN4924 attenuates BBB breakdown after ischemic stroke. a, b Representative images (a) and quantification (b) of Evans blue extravasation at 24 hours after stroke in mice treated with vehicle or MLN4924 (n = 8). c Representative in vivo multiphoton microscopic images of intravenously injected FITC-dextran (MW = 40 KDa) leakage from cortical vessels in sham-operated mice and ischemic mice treated with vehicle or MLN4924. Bar = 100 μm. d Quantification of the permeability (P) product of FITC-dextran for each group (n = 6). e Representative images of coronal brain sections showing the leakage of intravenously injected BSA into the brain. Bar = 1 mm. f Quantification of extravascular BSA fluorescence (n = 5). g Western blot assay for IgG levels in capillary-depletion brain tissue. h Quantification of IgG deposits in capillary-depletion brains (n = 5). i Representative images of IgG perivascular accumulation (green) and CD31-positive capillaries (white) in sham-operated mice and ischemic mice treated with vehicle or MLN4924. Bar = 10 μm. j Reduced tight junction protein ZO-1, occludin, and claudin-5 and adherens junction protein VE-cadherin levels in isolated brain microvessels of ischemic mice and reversal

by MLN4924 treatment. Data were analyzed using unpaired Student's t test and one-way ANOVA followed by Bonferroni multiple comparison test. Values are mean ± SD. * P < 0.05.

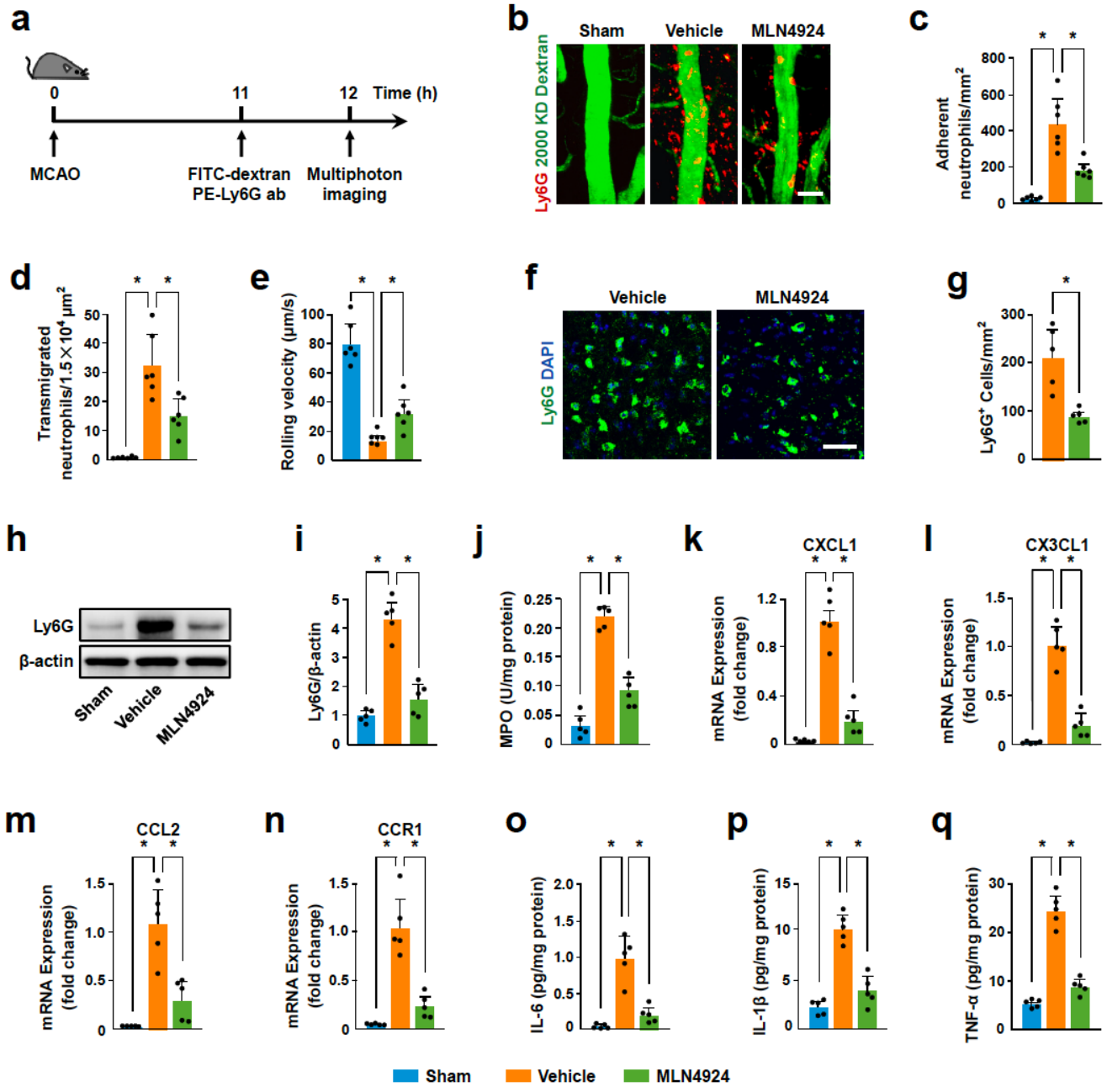

Figure 4

MLN4924 reduces neutrophil infiltration and proinflammatory cytokines expression in the ischemic brains. a Timeline of multiphoton microscopic experiments. PE-Ly6G ab, PE-conjugated monoclonal Ly6G antibody. b Representative in vivo multiphoton microscopic images of rolling and adherent neutrophils (red) inside the blood vessels (green) and of infiltrated neutrophils into the brain parenchyma. Bar = 40 μm. c-e Number of adherent neutrophils (c) and transmigrated neutrophils (d), and rolling velocity (e) in sham-operated mice and ischemic mice treated with vehicle or MLN4924 at 12 hours after stroke (n = 6).

f, g Representative images (f) and quantification (g) of Ly6G+ neutrophils at 24 hours (n = 6). Bar =30 μm. h, i Representative western blot (h) and quantification of the amount (i) of neutrophils in the ischemic brain in mice treated with vehicle or MLN4924 at 24 hours (n = 5). j Quantification of MPO activity in the brains of mice at 24 hours (n = 5). k-n Relative gene expression of CXCL1 (k), CX3CL1 (l), CCL2 (m) and CCR1 (n) in the brains of mice at 24 hours (n = 5). o-q Quantification of proinflammatory cytokines IL-6 (o), IL-1β (p) and TNF-α (q) by ELISA in the brains of mice at 24 hours (n = 5). Data were analyzed using one-way ANOVA followed by Bonferroni multiple comparison test and unpaired Student's t test. Values are mean ± SD. * P < 0.05.

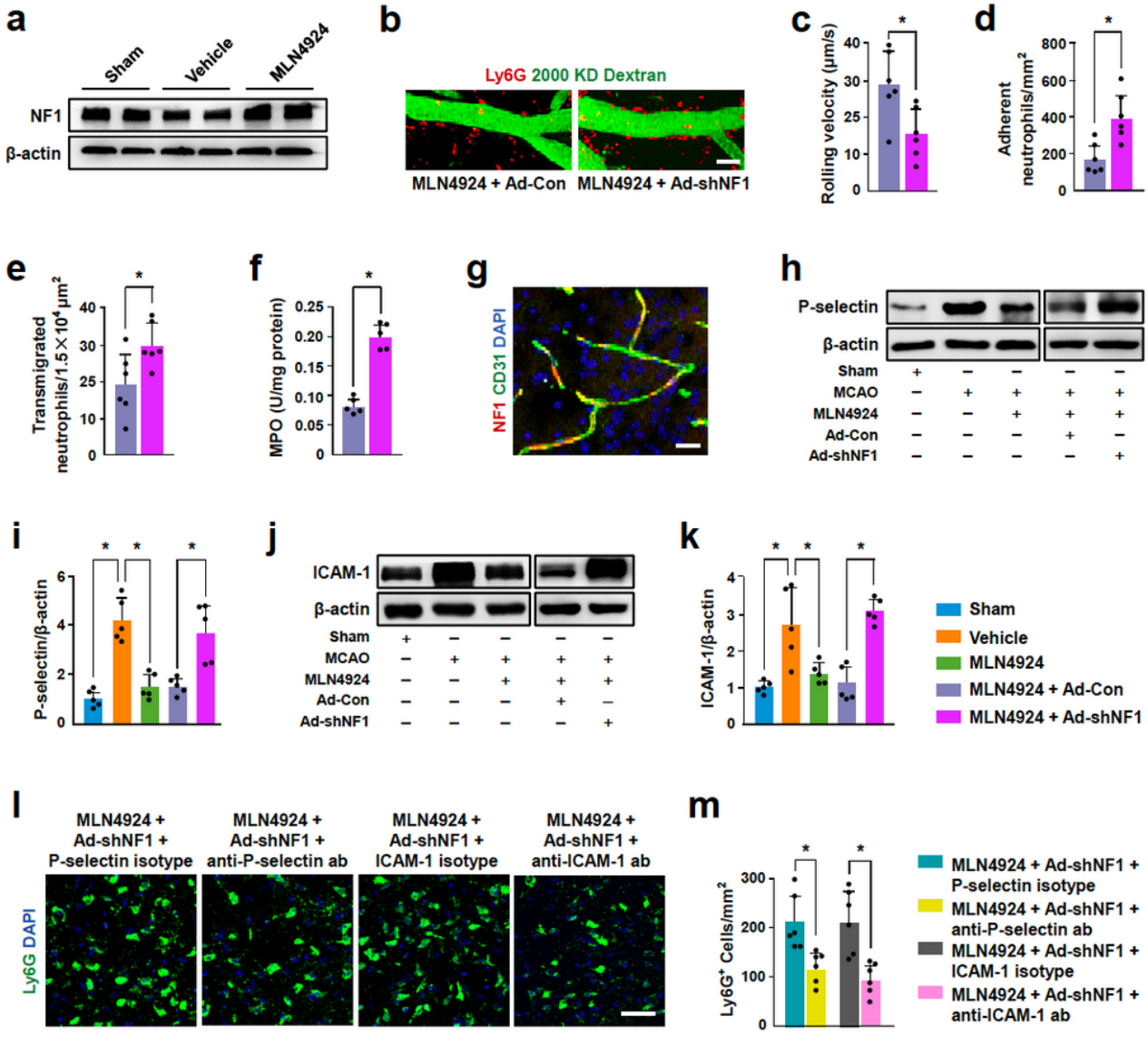

Figure 5

NF1 silencing abolishes MLN4924-dependent inhibition of neutrophil infiltration. a Representative immunoblots of NF1 levels in the ipsilateral hemisphere in sham-operated mice and ischemic mice treated with vehicle or MLN4924. b Representative in vivo multiphoton microscopic images of rolling and

adherent neutrophils (red) inside the blood vessels (green) and of infiltrated neutrophils into the brain parenchyma. Bar = 40 μm. c-e Rolling velocities (c), and number of adherent neutrophils (d) and transmigrated neutrophils (e) after injection of MLN4924 together with control adenovirus (Ad-Con) or NF1 shRNA (Ad-shNF1) (n = 6). f Quantification of MPO activity in the brains of mice (n = 5). g Representative confocal image showing NF1 (red) co-localization with CD31-positive endothelial cells (green) in the ischemic brains. Bar = 20 μm. h-k Representative immunoblots and quantification of P-selectin (h, i) and ICAM-1 (j, k) levels in isolated brain microvessels in sham-operated mice and ischemic mice treated with vehicle, MLN4924, MLN4924 and control adenovirus (Ad-Con) or MLN4924 and NF1 shRNA (Ad-shNF1). l, m Representative images (l) and quantification of Ly6G+ neutrophils (m). ab, antibody. Bar =30 μm. Data were analyzed using unpaired Student's t test and one-way ANOVA followed by Bonferroni multiple comparison test. Values are mean ± SD. * P < 0.05.

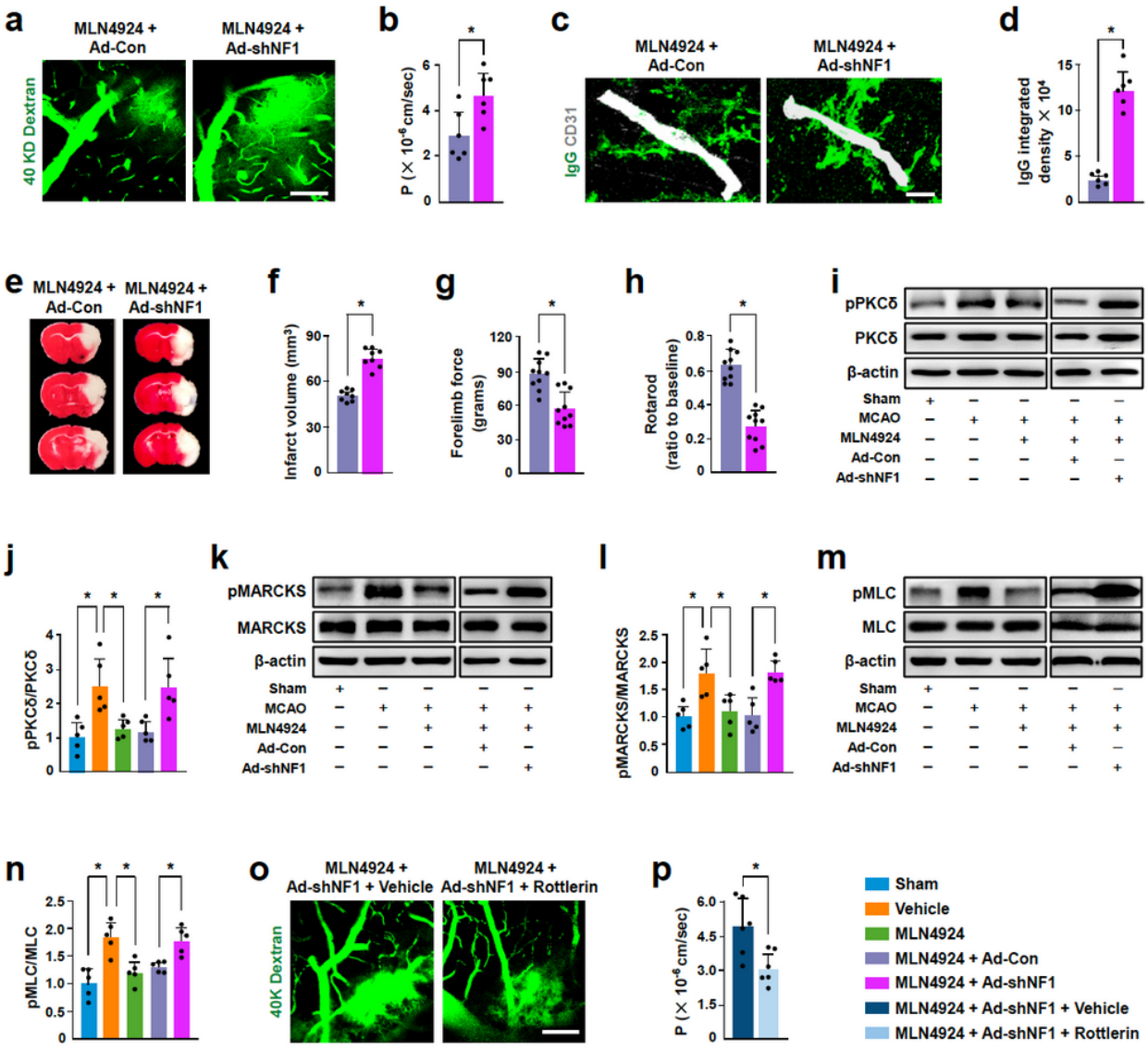

Figure 6

NF1 silencing blocks MLN4924-afforded BBB protection. a Representative in vivo multiphoton microscopic images of intravenously injected FITC-dextran leakage from cortical vessels in ischemic mice treated with MLN4924 and control adenovirus (Ad-Con) or MLN4924 and NF1 shRNA (Ad-shNF1) at 24 hours after stroke. Bar = 100 μm. b Quantification of the permeability (P) product of FITC-dextran for each group (n = 6). c Representative images of IgG extravascular deposits (green) and CD31-positive capillaries (white). Bar = 10 μm. d Quantification of IgG extravascular deposits (n = 6). e Representative photographs of TTC stained coronal brain sections showing larger cerebral infarct in mice treated with MLN4924 and NF1 shRNA (Ad-shNF1) than in mice treated with MLN4924 and control adenovirus (Ad-Con). f Quantitation of infarct volumes for each group (n = 8). g, h NF1 silencing worsened neurological outcomes in MLN4924-treated mice (n = 10). i, j Representative immunoblots (i) and quantification of pPKCδ (j) levels in sham-operated mice and ischemic mice treated with vehicle, MLN4924, MLN4924 and control adenovirus (Ad-Con) or MLN4924 and NF1 shRNA (Ad-shNF1) (n = 5). k, l Representative immunoblots (k) and quantification of pMARCKS (l) levels. m, n Representative immunoblots (m) and quantification of pMLC (n) levels. o Representative in vivo multiphoton microscopic images of intravenously injected FITC-dextran leakage from cortical vessels in MLN4924-treated mice after injection of vehicle or the PKCδ inhibitor rottlerin together with NF1 shRNA (Ad-shNF1). Bar = 100 μm. p Quantification of the permeability (P) product of FITC-dextran for each group (n = 6). Data were analyzed using unpaired Student’s t test and one-way ANOVA followed by Bonferroni multiple comparison test. Values are mean ± SD. * $P < 0.05$.

Supplementary Files

This is a list of supplementary files associated with this preprint. Click to download.

- SupplementaryFigures2021221.pdf